III International Conference on Particle-based Methods – Fundamentals and Applications
PARTICLES 2013
M. Bischoff, E. Oñate, D.R.J. Owen, E. Ramm & P. Wriggers (Eds)

RECENT DEVELOPMENTS IN PARTICLE-BASED METHOD FOR SIMULATION OF EXPLOSIVE BLAST

Carlos Bonifasi-Lista[1], Rebecca M. Brannon[2] James E. Guilkey[3]

[1] Department of Mechanical Engineering, University of Utah
50 S. Central Campus Dr., Room 2110, Salt Lake City, UT, 84112
carlos.bonifasi@utah.edu

[2] Department of Mechanical Engineering, University of Utah
50 S. Central Campus Dr., Room 2202, Salt Lake City, UT, 84112
Rebecca.Brannon@utah.edu
http://csmbrannon.net/

[3] Schlumberger Technology Corporation
1935 South Fremont Drive
Salt Lake City, UT 84104
jguilkey@slb.com

Key words: Material Point Method, CPDI, Meshfree Methods, Large velocity gradients, error analysis, boundary tractions

Abstract. To support simulations of blast loading from explosives using the Material Point Method (MPM), preliminary studies of gas expansion in MPM using the recently developed Convected Particle Domain Interpolation (CPDI) integrator, as well as established integrators based on the Generalized Interpolation Material Point (GIMP) method, show that prevailing algorithms for updating the deformation gradient produce results that are often grossly inconsistent with the update of the particle positions. Mapping of velocity to boundary background nodes is analyzed and demonstrated to induce large errors in problems involving large velocities and rapidly changing velocity gradients (common in blast and penetration applications). The error in the velocity cascades to ultimately corrupt other variables, especially the velocity gradient and stress on which it depends. A well-respected code verification process (the method of manufactured solutions) is used to quantify the errors in the update of variables in the MPM using the CPDI interpolator. Different methods based on linear extrapolation were tested for their potential to improve the mapping of the large-deformation velocity fields in blast and penetration, but with only isolated successes in some cases that often worsened results in other cases.

1 MOTIVATION

Applications of the Material Point Method (MPM) [2] to oil well-bore perforation by shaped charged jet show anomalously large deviations in the deformation gradient near free surfaces with highly stressed particles. To better understand this problem, a set of 1D blast simulations using different interpolators were performed. Each simulation consists of two materials, the explosive and an adjacent aluminum flyer. The detonation starts at the left. The gas resulting from the detonation expands to the right and left. The aluminum flyer is accelerated by the gas expansion. Figure 1 shows that the values of the deformation gradient F near the left (free) boundary are extremely sensitive to the choice of MPM interpolator.

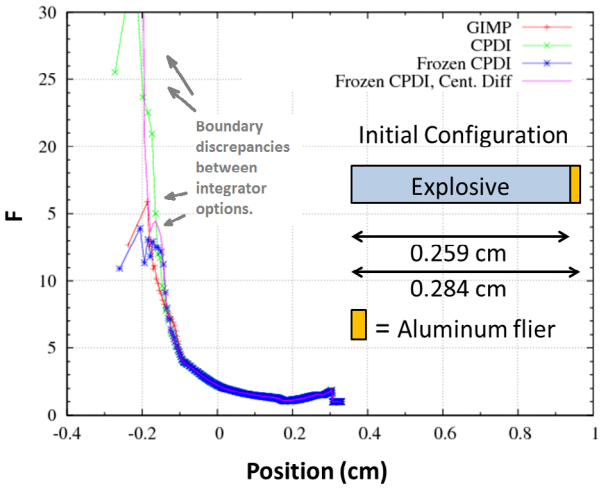

Figure 1: Snapshot of the deformation gradient F using different interpolators for a 1D blast simulation: GIMP (Generalized Interpolation Material Point Method); CPDI (Convected Particle Domain Interpolation Method); Frozen CPDI (which limits excessive growth/distortion of the particle domain), Frozen CPDI-Cent.Diff (which is a form of Frozen CPDI that sets the deformation gradient to its exact value based on separation of nearest particles.

2 ALGORITHM FOR CPDI

We focus on kinematic errors in the Convected Particle Domain Interpolator (CPDI) algorithm, which has been demonstrated to have superior accuracy and convergence properties over other material point methods [1]. We summarize the 1D algorithm for CPDI as described in [1]. Variables for particles and background nodes are subscripted with p (particle number) and i (node number), respectively. An upper-script n is the time step. To begin, the mass m and velocity v at time n are mapped from particles to the grid:

$$m_i^n = \sum_p \phi_{ip}^n m_p \qquad v_i^n = \frac{\sum_p \phi_{ip}^n m_p v_p^n}{m_i^n} , \tag{1}$$

where ϕ_{ip}^n is the average of the i^{th} nodal shape function on the grid averaged over the p^{th} particle domain, which is evolved to first order accuracy by the CPDI method as deformation proceeds (e.g., the particle domain might evolve from a rectangle to a parallelogram). Particle mass is conserved $m_p^{n+1} = m_p^n = m_p$. External and internal forces at grid node i are defined by:

$$f_i^{\text{ext}^n} = \sum_p \int_{\partial\Omega_p^n} t^n \phi_i^n dS + \sum_p \phi_{ip}^n b_p^n m_p \qquad f_i^{\text{int}^n} = -\sum_p \nabla\phi_{ip}^n \cdot \sigma_p^n V_p^n \ . \tag{2}$$

Here, $\partial\Omega_p^n$ is the intersection of the physical boundary with the particle boundary (which is a non-empty set only for particles abutting the boundary), T^n is the boundary traction acting on $\partial\Omega_p$, and b_p^n is the body force acting on particle p, σ_p^n is the stress of the particle, V_p^n is the particle volume (which, in 1D, is the length). With grid forces thus known, the nodal acceleration and explicitly updated velocity are

$$a_i^n = \frac{f_i^{\text{int}^n} + f_i^{\text{ext}^n}}{m_i^n} \qquad \text{and} \qquad v_i^{n+1} = v_i^n + a_i^n \Delta t \ . \tag{3}$$

The particle position and velocity are updated by

$$x_p^{n+1} = x_p^n + \sum_i \phi_{ip} v_i^{n+1} \Delta t \qquad \text{and} \qquad v_p^{n+1} = v_p^n + \sum_i \phi_{ip}^n a_i^n \Delta t \ . \tag{4}$$

Velocity gradient and the deformation gradient at each particle are updated using

$$\nabla v_p^{n+1} = \sum_i \nabla\phi_{ip} v_i^{n+1} \qquad \text{and} \qquad F_p^{n+1} = (1 + \nabla v_p^{n+1} \Delta t) F_p^n \ . \tag{5}$$

Volume V and density ρ of particles is updated using

$$V_p^{n+1} = J_p^{n+1} V_p^0 \qquad \text{and} \qquad \rho_p^{n+1} = \left(J_p^{n+1}\right)^{-1} \rho_p^0 \ . \tag{6}$$

Here, J_p^{n+1} is the determinant of the deformation gradient at time step $n+1$.

3 ANALYSIS OF THE KINEMATICS

It is not known which of the conflicting solutions in Fig. 1, if any, is close to the real deformation gradient, which motivates our investigating this problem by using the method of manufactured solutions (MMS) to obtain a 1D adiabatic expansion to assess the accuracy of MPM and to perform a kinematic analysis. Basically, MMS allows constructing a problem from a given analytical solution.

For simplicity, we start with a displacement function u and corresponding mapping function for the current position x given by

$$u = \beta t X \tag{7}$$

$$x = X + u = X(1 + \beta t) \qquad \text{for } X \in [0.2, 1.2] \ . \tag{8}$$

Here, X is the position coordinate in the initial configuration. Taking derivatives, the velocity and acceleration of the particles are

$$v = \frac{Dx}{Dt} = \beta X \tag{9}$$

The resulting acceleration a is zero. The deformation gradient F is

$$F = \left(\frac{\partial x}{\partial X}\right)_t = 1 + \beta t \ . \tag{10}$$

For 1D adiabatic expansion, the momentum equation reduces to

$$\sigma_{,x} + b\rho = a\rho \ , \tag{11}$$

where $\sigma_{,x}$ is the partial derivative of stress σ with respect to x holding t constant, and ρ is the lineal mass density. We assume a simple 1D constitutive model:

$$\sigma = P_0(F^{-1} - 1) \ . \tag{12}$$

For this manufactured solution, the displacement field is linear with respect to X, and hence F is spatially uniform. Therefore, taking the material to be homogeneous (i.e., $P_{0,x} = 0$), it follows from the constitutive model that $\sigma_{,x} = 0$. Thus, since $a = 0$, the body force field is zero, making boundary tractions the only forcing function. Using the constitutive model, the boundary traction is $T = P_0(F_{\rm MS}^{-1} - 1)$, where the subscript MS stands for manufactured solution in Eq. (10).

3.1 KINEMATIC ANALYSIS OF 1D LINEAR ADIABATIC EXPANSION

For the the 1D MMS, we consider the particle placements shown in Fig. 2. The initial mapping of the masses and velocities from the particles to the background nodes is

$$m_1^0 = m_p \qquad\qquad v_1^0 = \frac{3}{4}v_{p1}^0 + \frac{1}{4}v_{p2}^0 \tag{13}$$

$$m_2^0 = 2m_p \qquad\qquad v_2^0 = \frac{1}{8}v_{p1}^0 + \frac{3}{8}v_{p2}^0 + \frac{3}{8}v_{p3}^0 + \frac{1}{8}v_{p4}^0 \ . \tag{14}$$

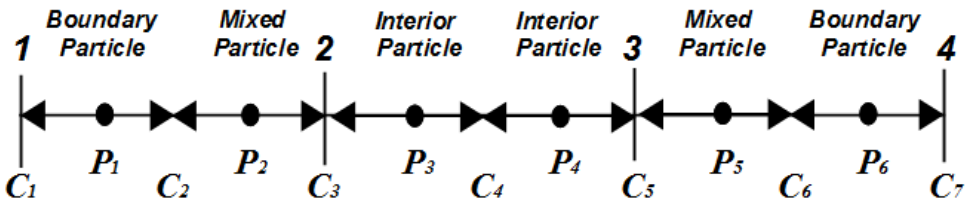

Figure 2: 1D particle distribution composed of 3 background cells and two particles per cell. The P_i labels are placed at particle centers, while C_i stands for the endpoints (corners) of particle domains. In 1D, the domain of neighboring particles cannot separate in CPDI. Background nodes are denoted by numbers 1-4. The original length of each particle domain is denoted $2r_0$.

Here, m_p is the mass of the particle that it is assumed to be constant and equal for every particle. Making use of the manufactured solution, the error in the velocity v_1^0 at node 1 at time step 0 is:

$$v_{1_{\text{error}}}^0 = v_{1_{\text{MS}}}^0 - v_1^0 = -\frac{3\beta}{2} r_0 \ . \tag{15}$$

Therefore, there is an error directly proportional to parameter β that controls the velocity gradient and proportional to the initial particle length ($2r_0$) of particle domain in the mapping of the information to the background node 1. For this manufactured solution, velocity at boundary node 1 will be overestimated at the very first time step. There is not error associated with the velocity of node 2 at time step 0. By symmetry considerations, $m_4^0 = m_1^0$ and $m_3^0 = m_2^0$. Velocity at node 3 has no error and velocity at node 4 has an error of $3\beta r_0/2$. Therefore, the velocity at node 4 at time step 0 will be overestimated.

At time step 0, the deformation gradient is 1 and therefore, the boundary tractions and the internal forces are zero and automatically, the accelerations at the background nodes are zero (Eq. 3). Now, the kinematic variables at the background nodes need to be updated. Because of no acceleration, the velocity at background nodes at time step 1, are given by Eq. (3) to be the same velocities at previous time step:

$$v_i^1 = v_i^0 \qquad \text{for } i = 1, 2, 3, 4 \ . \tag{16}$$

Using Eq. (4), velocities at the particles at time step 1 are

$$v_{pi}^1 = v_{pi}^0 = \beta X_{pi} \qquad \text{for i=1...6} \ . \tag{17}$$

Here, X_{pi} denotes the initial position of the center of particle P_i. There is no error in the update of the velocities at the center of the particles at time step 1.

Applying Eq. (5), the update of the velocity gradients at the particles is

$$\nabla v_{pi}^1 = \frac{5}{8}\beta \qquad \text{for i=1,2,5,6} \tag{18}$$

$$\nabla v_{pi}^1 = \beta \qquad \text{for i=3,4} \ . \tag{19}$$

The manufactured velocity gradient is constant and equal to β. Therefore, boundary particles (P_1, P_6) and mixed particles(P_2, P_5) have an error in the update of the velocity gradient of $3/8 = 37.5\%$. There are no errors in the update of the velocity gradient for the interior particles (P_3, P_4) at time step 1.

The update of the deformation gradient depends on the gradient of the velocity (Eq. 5). Therefore, the deformation gradient at time step 1 is

$$F_{pi}^1 = (1 + \nabla v_{pi}^1 \Delta t) F_{pi}^0 = 1 + \frac{5}{8}\beta\Delta t \qquad \text{for i = 1,2,5,6} \tag{20}$$

$$F_{pi}^1 = (1 + \nabla v_{pi}^1 \Delta t) F_{pi}^0 = 1 + \beta\Delta t \qquad \text{for i = 3,4} \ . \tag{21}$$

The manufactured solution is $1 + \beta\Delta t$. Therefore, there is no error in the update of the deformation gradient for the interior particles (P_3,P_4). However, there is an error in the boundary and mixed particles. The relative error is given by:

$$F_{\text{RelativeError}} = \frac{|F - F_{MS}|}{F_{MS}} = \frac{\frac{3}{8}\beta\Delta t}{1 + \beta\Delta t} \, . \tag{22}$$

The relative error goes to zero as $\Delta t \to 0$, and it has an upper bound of $3/8 = 37.5\%$ as $\Delta t \to \infty$, which occurs in the first time step for boundary and mixed particles.

Summarizing our findings, the mapping in the very first time step of the velocities from the particles to the background nodes has an error associated with the boundary nodes. Interior nodes have no error. Equation (13) reveals that the mapping of velocity from particles of boundary nodes is an interpolation. However, the MS given by Eq. (9) indicates that velocity is linear function of the initial position X. Therefore, the resulting velocity at background node 1 lies between the velocities of particles 1 and 2 when it ought to lie outside. This does not happen in the mapping of velocities from particles to interior nodes as given in equation (14) at time step 1. But this is just a consequence of imposing zero acceleration (by design) for this highly simplified MS. In general, there will be errors even in the interior.

The boundary and mixed particles have 37.5% error in their velocity gradients in the first time step. This error affects the update of the deformation gradient, which then induces error in the constitutive update of stresses (σ). This in turn will affect the calculation of the accelerations of the background nodes. At this point, the errors in the acceleration will aggravate errors in the update of position and velocity of particles.

4 SIMULATIONS

This analytical study quantifies the errors in the update of the kinematic variables for the first time step for CPDI. It is very hard to analytically quantify how the errors propagate with time. In this section, we will show numerically how the error propagates for the manufactured solution introduced previously. All simulations are run for 20 µs and parameter β that represents the velocity gradient is set to 10^5s^{-1}. Initially there are 4 particles per background cell.

Figure 3 shows the deformation gradient and how the error at the boundary cells propagates after 20 µs. The relative error at the boundary particles reaches 38.29 % and decreases as we walk towards the interior nodes. Relative errors in the update of velocity, position of particles and deformation gradient are shown in Fig. 4. Even though the errors in the deformation gradient are very large near the boundaries, the maximum relative error for velocity and position of particles are 2.09 % and 6.08 % respectively and occurs at the boundary particles.

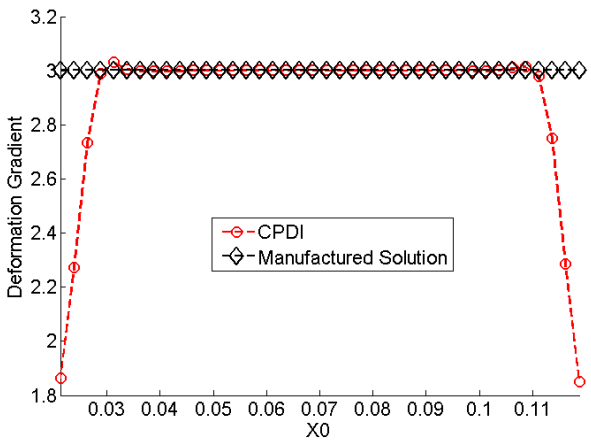

Figure 3: Snapshot of the deformation gradient of particles at time 20.018 µs. $P_0 = -10^{-2}$MPa.

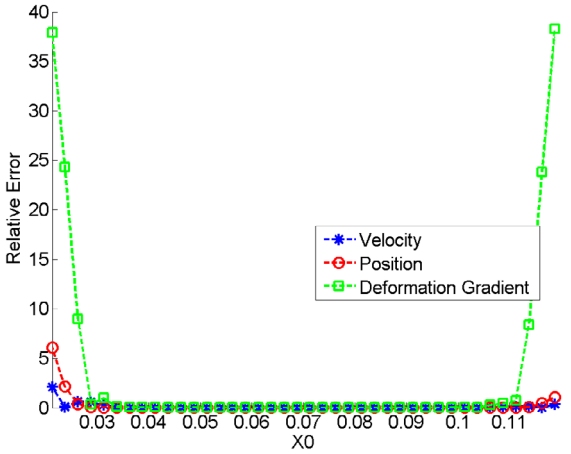

Figure 4: Relative errors at time 20.018 µs. $P_0 = -10^{-2}$MPa.

From the manufactured solution, we know that acceleration should be zero for all time steps, but there is an error evident in Fig.5. This error comes from errors in the update of stresses equation (12) that depends on the deformation gradient. The errors in the update of the deformation gradient propagate in the calculation of the interior forces and hence, cascade to the update of the acceleration through the rate of momentum equation.

So far, in the simulations presented, the particles are subject to relatively low stresses. The level of stress in the particles depends on the parameter P_0 in Eq. (12). The easy way to address the influence of the constitutive model in the errors in the kinematics through the update of the interior forces is to change P_0 in (12). We run simulations with $P_0 = 100$ MPa. This has the effect of stiffening the gas. Fig. 6 shows how the error in the deformation gradient spreads faster through the interior nodes as particles are more stressed. Relative errors in the update of velocity and position are shown in Fig. 7. The error in the update of stresses affects the kinematics via Eq. (2). As a consequence of the errors in the update of the interior forces, acceleration in particles reaches values of the order of 10^8 m s^{-2} when it is supposed to be zero. In the previous example, when $P_0 = 0.01$MPa, the particle accelerations reach values of the order of 10^6 instead. In all simulations, the CFL number was 0.1 to determine the time step. Even with CFL number set to 0.001, the results did not change eliminating numerical instabilities as the cause of the increase of the error. The time step was determined as:

$$dt = \mathrm{CFL}\frac{\mathrm{h_y}}{\mathrm{c} + \mathrm{MaxV}} \ . \tag{23}$$

here, c is the speed of the wave and MaxV is the maximum particle velocity. $\mathrm{h_y}$ represents the initial length of particle domain. The problem is an expansion, so $\mathrm{h_y}$ will be always equal or small than particle length in subsequent time steps.

Velocity gradients are always positive, so there is no shock wave and hence, the oscil-

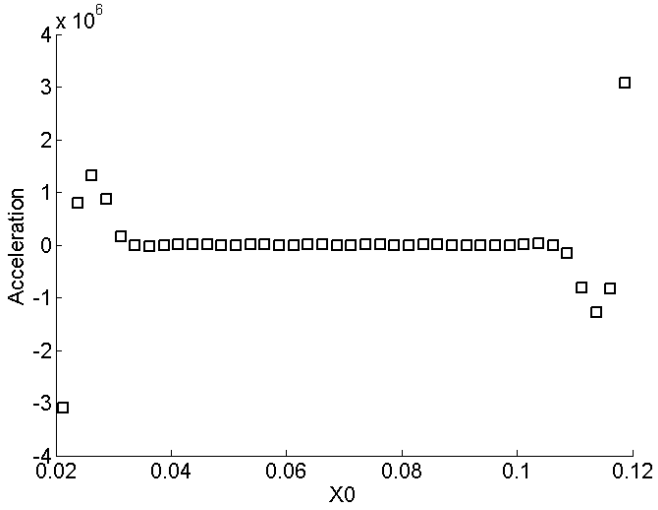

Figure 5: Acceleration of the particles at time 20.018 µs. $P_0 = -10^{-2}$MPa.

lations in our simulation are not be smoothed out adding artificial viscosity. Artificial viscosity helps in the presence of large negative gradients of velocity, as in shock wave propagation.

5 NONLINEAR ADIABATIC EXPANSION

In the previous sections, a linear manufactured solution was introduced. The simplicity of it allows analytically quantifying errors in the kinematics in the first time steps. In this section, a nonlinear manufactured solution is obtained and compared against the MPM algorithm. Specifically, the nonlinear mapping is

$$x = X + u = X + \beta t \left(L^2 X - \frac{X^3}{3} \right) \qquad \text{for } X \in [-L, L] \, . \tag{24}$$

Here, L is half length of the continuum domain. From this mapping, the velocity and velocity gradient are

$$v = \beta \left(L^2 X - \frac{X^3}{3} \right) \qquad \nabla v = \beta \left(L^2 - X^2 \right) \, . \tag{25}$$

The deformation gradient is

$$F = 1 + \beta t \left(L^2 - X^2 \right) \, . \tag{26}$$

By design, this problem has a zero velocity gradient at the boundary ($X = \pm L$), and there is no deformation at the boundaries, making this a free boundary problem. The constitutive equation is the same as the one used in the linear case: Eq. (12). Following

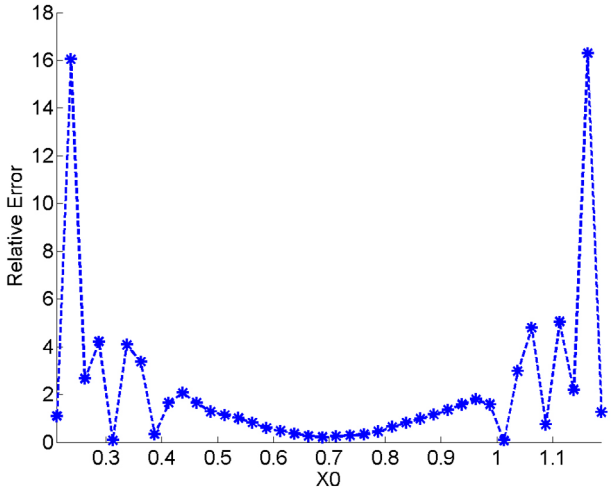

Figure 6: Relative Error (%) of deformation gradient at time 20.013 µs. $P_0 = -100$MPa.

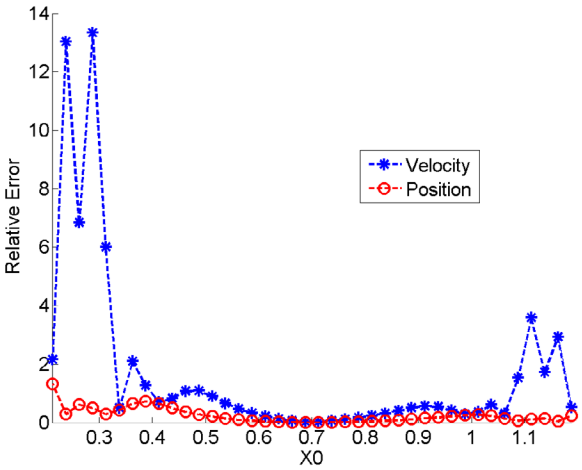

Figure 7: Relative Error (%) in velocity and position of particles at time 20.013 µs. $P_0 = -100$MPa.

the procedure described in the previous section, the acceleration of particles is zero, and the body force is given by

$$b = 2\beta P_0 \rho_0 t F^{-2} X \ . \tag{27}$$

where ρ_0 is the initial particle density. Analytical solution of the kinematics, as performed for the linear case, is not possible for this nonlinear case. Instead, we present MPM simulations and compare the results with the manufactured solution.

Parameter β was set to 10^8 in the simulations and the initial domain is $[-0.1, 0.1]$. Because of symmetry in the manufactured solution, only half of the domain is shown in the figures. The deformation gradient shows large errors near the boundary as shown in Figs. 8 and 9. Errors in the update of the deformation gradient reach 20% while errors in velocity and position of particles reach 9% and 2% respectively. Velocity and position distributions are shown in Figs. 10 and 11. If the gas is stiffened by setting $P_0 = 100$ MPa, the errors in the kinematics spread and increase noticeably.

6 NUMERICAL IMPROVEMENT OF THE MAPPING OF VELOCITY FROM PARTICLES TO BACKGROUND BOUNDARY NODES

The analysis showed that all the errors initially are originated from the mapping of velocity of particles to the background boundary nodes. The problem is reduced to the fact that the mapping to the background boundary nodes is an interpolation and this will underestimate or over estimate velocities at the background nodes. This error triggers errors in the rest of kinematic variables affecting mostly the update of the deformation gradients and hence, the update of stresses through the constitutive equation. Figures 12 and 13 show two cases of particle distribution at the boundary cell with the velocity at the background node i based on the particle distribution. It is easily seen that, in both

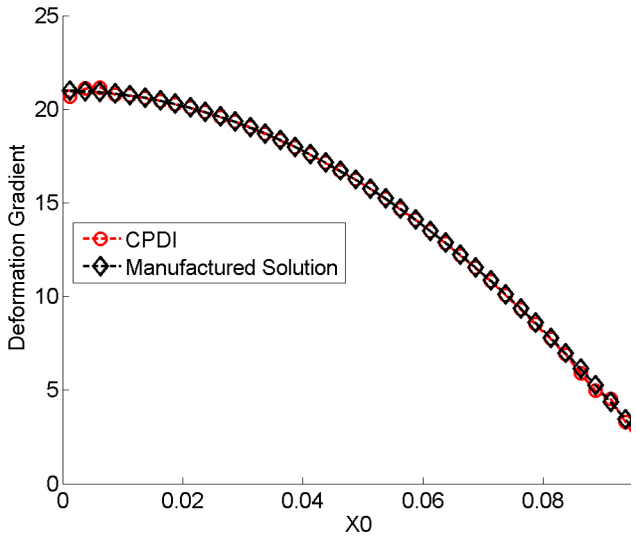

Figure 8: Deformation gradient at time 20.005 µs. $P_0 = -1$MPa

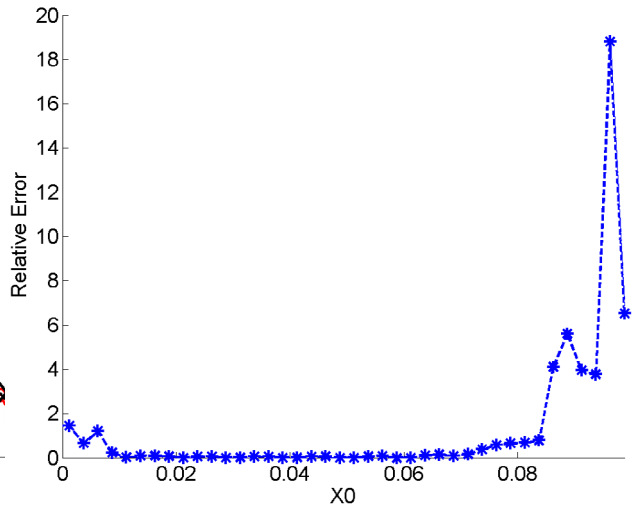

Figure 9: Relative Error (%) in deformation gradient at time 20.005 µs. $P_0 = -1$MPa.

cases, the velocity at the node i will be underestimated.

In this section, we will present some methods that might help to minimize the error in the mapping of velocity to the background nodes and test them for the nonlinear manufactured solution. Wallstedt and Guilkey [3] present a gradient enhancement method that, for their case studies, successfully improved the mapping of velocity to the background nodes for MPM and GIMP. The method can also be applied to CPDI. It consists first in extrapolating the velocity of the particles to the nodes as:

$$v_{ip}^{e} = v_p - \frac{\partial v_p}{\partial dx}(x_p - x_i) \ . \tag{28}$$

Then v_{ip}^{e} is used in Eq. (4) instead of v_p to set the velocities in the background nodes.

The second method creates artificial particles from the boundary particle to the boundary node or beyond it in each time step. Velocity at the boundary particles is extrapolated to these artificial particles using Eq. (28). Then, Eq. (4) (with i replaced by p_e, where p_e stands for the particle ID number of these extra particles) is used to assign velocities to these particles, and they are used along with the rest of the particles to determine velocities in the background nodes. Then the assigned velocity of the artificial particles along with the velocity of the particles are used in Eq. (4) to determine the velocity of the background nodes. We ran simulations using two different methods to create artificial cells. The first method, named AP1, creates artificial particles to fill the boundary cell. In the second method, named AP2, artificial particles were created to fill the boundary cell and an extra cell. Looking at Fig. 14, the first method would fill the boundary cell with artificial particles until node 1 and the second method until node 2. Fig. 15 shows the results in the determination of the deformation gradient for the nonlinear manufactured

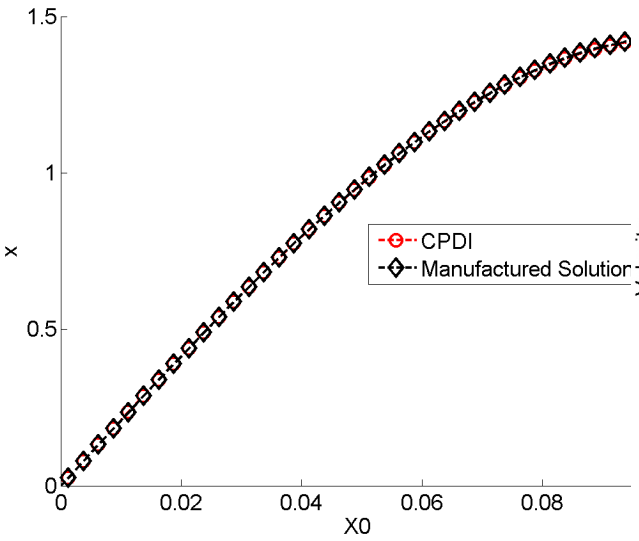

Figure 10: Position of particles at time 20.005 µs. $P_0 = -1$MPa

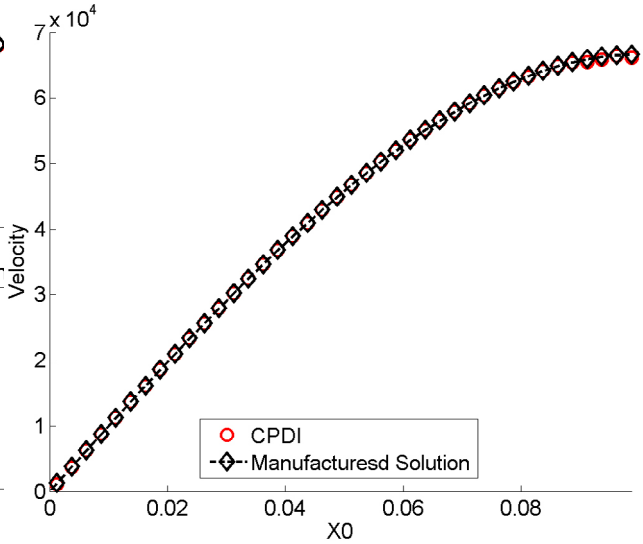

Figure 11: Velocity of particles at time 20.005 µs. $P_0 = -1$MPa.

solution described in previous section. In general, for this manufactured solution, there is no improvement at all. If the particles are stressed further by increasing the parameter P_0 in the constitutive equation, the update of the kinematics worsen drastically.

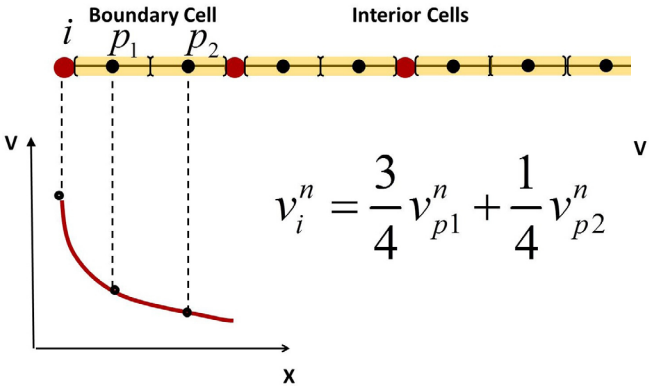

Figure 12: Illustrative example of particle distribution in the boundary node. Large and small dots represent background nodes and particle's center respectively.

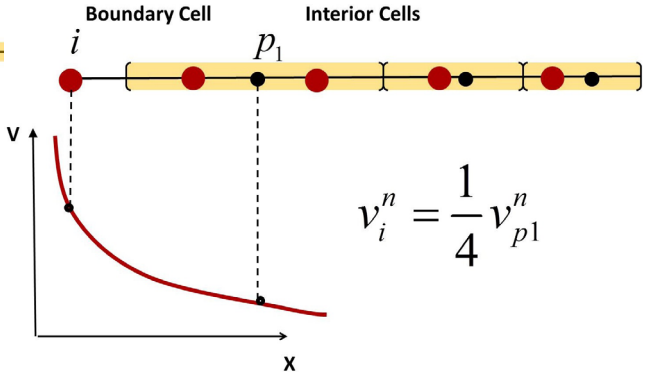

Figure 13: Illustrative example of particle distribution in the boundary node. Large and small dots represent background nodes and particle's center respectively.

7 CONCLUSIONS

In this paper we have quantified errors in traction and free boundary problems subjected to large velocity and large velocity gradients at the boundaries. We have shown how these errors can increase dramatically and propagate to interior nodes depending

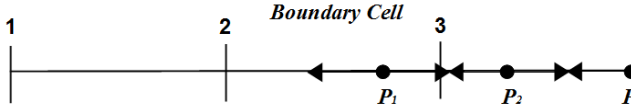

Figure 14: Illustrative example of particle distribution in the boundary node. Numbered vertical bars represent the background nodes and the dots represent the center of particles and the arrows are their boundaries.

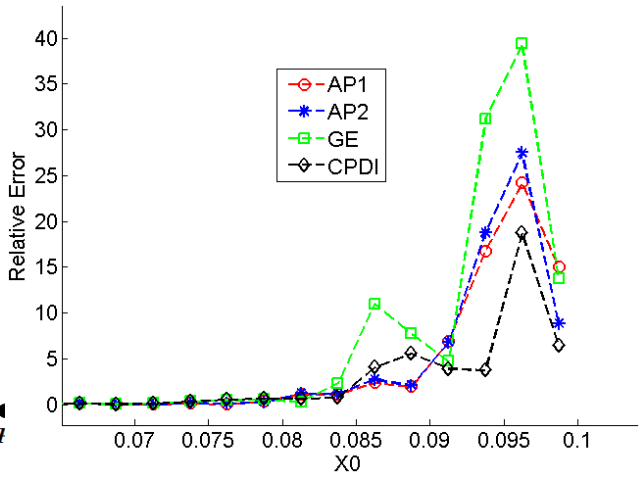

Figure 15: Error in deformation gradients using different gradient enhancement methods. AP stands for artificial partical method. GE for gradient enhancement; $P_0 = 1$MPa and $\beta = 10^8$.

on the constitutive equation. The errors in the deformation gradient and the update of stresses are of a higher order than the errors in the updated of kinematic quantities such as velocity and position. Different enhancement methods were used to try to smear out the error with only mixed success. Therefore, the issue of boundary kinematics errors (with associated errors cascading into the interior) remains an open and essentially unsolved problem that is likely to adversely affect accuracy of well-bore perforation simulations where naturally free boundary with high stress particles appear.

Acknowledgements: Support for this work by Schlumberger Corporation and the Office of Naval Research is gratefully acknowledged. The need for this research was first identified in penetration and blast simulations that were run using resources of the University of Utah's Center for High Performance Computing (CHPC).

REFERENCES

[1] Sadeghirad, A. and Brannon, R.M. and Burghardt, J. A convected particle domain interpolation to extend applicability of the material point method for problems involving massive deformations. *Int. J. Num. Meth. Engng.* (2011) **86**:473-480.

[2] Sulsky, D. and Zhou, S.J. and Schreyer, H.L. Application of particle-in-cell method to solid mechanics. *Comput. Phys. Commun.* (1995) **87**:236-252.

[3] Wallstedt, P.C. and Guilkey, J.E. Improved Velocity Projection for the Material Point Method. *CMES* (2007) **19**: 223-232.